

Enabling Distributed Medium Access Control for Impulse-Based Ultrawideband Radios

Nathaniel J. August, *Member, IEEE*, Hyung-Jin Lee, *Member, IEEE*, and Dong Sam Ha, *Senior Member, IEEE*

Abstract—Impulse-based ultrawideband (I-UWB) is an attractive radio technology for large *ad hoc* and sensor networks due to its robustness to multipath effects, subcentimeter ranging ability, simple hardware, and low radiated power. Large distributed networks, such as *ad hoc* and sensor networks, often implement distributed medium access control (MAC) protocols based on carrier sense multiple access (CSMA). In CSMA, narrowband systems check for medium activity before transmitting by checking for in-band energy around a carrier frequency. I-UWB systems lack a carrier, and the narrow pulses, low radiated power, harsh channel conditions, and strict Federal Communications Commission power limits present challenges in detecting medium activity. We propose a pulse sensor for I-UWB systems that overcomes the challenges of quickly, reliably, and efficiently identifying medium activity. The pulse sensor enables distributed MAC protocols for I-UWB radios that are analogous to CSMA for narrowband radios. Simulations show that the proposed pulse sensor architecture is practical for I-UWB radios.

Index Terms—*Ad hoc* networks, carrier sense, medium access control (MAC), sensor networks, ultrawideband (UWB).

I. INTRODUCTION

SINCE the Federal Communications Commission's (FCC) historic allocation of spectrum in 2002, ultrawideband (UWB) radio communication has attracted an enormous amount of interest from scientific, commercial, and military sectors [1]–[4]. Ongoing developments in wireless technology and embedded systems have also spawned extensive research in wireless *ad hoc* and sensor networks [5], [6].

For *ad hoc* and sensor networks, an impulse-based UWB (I-UWB) radio has several advantages over narrowband radios [7]. First, the low radiated power is at least an order of magnitude less than typical narrowband radios [8], [9]. This leads to advantages such as low probability of detection and intercept, reuse of existing spectrum, minimal impact to existing users, and low transmit power [10]. Next, the wide bandwidth enables an extremely high data rate, which can be traded for longer range or more robust operation [11]. The wide instantaneous bandwidth also enables fine time resolution for use in radar, imaging, and ranging. Resilience to harmful multipath effects permits placement of I-UWB radios in areas inhospitable to narrowband systems, such as inside metal ship hulls [2]. The

ranging ability allows nodes to accurately discern location (subcentimeter ranging is possible), which can be an important service for applications and network protocols [12], [13]. Finally, the carrierless nature of I-UWB gives it the potential for simple low-power low-cost circuit implementations without intermediate oscillators and mixers [14].

To scale to a large number of nodes, *ad hoc* and sensor networks generally adopt distributed medium access control (MAC) protocols [8], [9], [15]–[17]. A popular distributed MAC protocol is carrier sense multiple access (CSMA) [18]. Before transmitting in CSMA, nodes must check for medium activity via carrier sense, which is also known as clear channel assessment (CCA). Narrowband systems implement CCA by checking for in-band energy around a carrier, but I-UWB systems have no carrier. The narrow pulses, low radiated power, harsh channel conditions, and strict FCC power limits further complicate CCA for I-UWB systems.

This paper proposes a pulse sensor that overcomes the challenges of detecting I-UWB medium activity. To operate similarly to narrowband carrier sense, the pulse sensor should detect medium activity in unknown channel conditions for I-UWB signals with unknown phase (i.e., noncoherent detection), unknown modulation, and unknown received energy level. Further, the implementation should meet three critical goals: 1) quick detection within a few symbols, 2) reliable detection with a low probability of false alarm and high probability of detection, and 3) efficient detection with moderate hardware complexity [16]. The proposed pulse sensor meets these goals and enables distributed MAC protocols for I-UWB that are analogous to CSMA in narrowband systems. In another work, we describe these MAC protocols for I-UWB [19].

This paper focuses on the pulse sensor. Section II describes relevant I-UWB characteristics. It also reviews existing methods to perform CCA in I-UWB, and it examines existing MAC protocols for I-UWB and for large *ad hoc* and sensor networks. Section III describes our proposed pulse sensor, and Section IV presents simulation results. Section V concludes this paper.

II. PRELIMINARIES

A. I-UWB

1) *Signaling*: A narrowband radio modulates data onto a carrier signal to occupy a narrow frequency band of a few kilohertz to a few megahertz, and the signal is continuous in time. The unique signaling of I-UWB represents the dual of narrowband signaling [1], [2]. A sharp pulse may occupy from 500 MHz to several gigahertz of spectrum, but it only lasts for

Manuscript received November 12, 2005; revised March 30, 2006 and May 23, 2006. The review of this paper was coordinated by Prof. X. Shen.

The authors are with the Virginia Tech VLSI for Telecommunications (VTVT) Laboratory, Bradley Department of Electrical and Computer Engineering, Virginia Tech, Blacksburg, VA 24061 USA (e-mail: nate_august@yahoo.com; hlee@vt.edu; ha@vt.edu).

Digital Object Identifier 10.1109/TVT.2007.895486

hundreds of picoseconds. The pulse is repeated in a pulse train at a pulse repetition interval (PRI) that lasts from nanoseconds to microseconds.

Two popular modulation schemes for I-UWB are orthogonal pulse-position modulation (PPM), which results in the same signal constellation as frequency shift keying in narrowband systems; and binary antipodal amplitude modulation, which results in the same signal constellation as binary phase-shift keying (BPSK) in narrowband systems. For PPM, a single pulse can represent multiple bits or chips. If there are N_s pulse positions, then the signal represents $\log_2 N_s$ chips or bits.

For a train of I-UWB pulses, spectral lines appear at integer multiples of the pulse repetition frequency (PRF) or $1/\text{PRI}$. Spectral lines are explained by examining the power spectral density (PSD) of an I-UWB signal. For any linear modulation, such as BPSK, pulse amplitude modulation, or ON-OFF keying (OOK), the PSD (Φ_{ss}) can be expressed as [20]

$$\Phi_{\text{ss}}(f) = \frac{\sigma_i^2}{T_f} |P(f)|^2 + \frac{\mu_i^2}{T_f^2} \sum_{m=-\infty}^{\infty} \left| P\left(\frac{m}{T_f}\right) \right|^2 \delta\left(f - \frac{m}{T_f}\right) \quad (1)$$

where δ is the impulse function, $P(f)$ is the Fourier transform of the pulse shape $p(t)$, T_f is the PRI, μ_i is the mean of the information sequence, and σ_i^2 is the variance of the information sequence. From the second term of (1), the spectrum contains discrete frequency components spaced every $1/T_f$, if $\mu_i \neq 0$. A similar analysis holds for a PPM scheme with N_s pulse positions of width T_p and probability p_k of a pulse appearing in position k ($0 \leq k \leq N_s - 1$), which has a PSD of [21]

$$\Phi_{\text{ss}}(f) = \frac{1}{T_f} |P(f)|^2 \left\{ 1 - |\Phi_{\text{ii}}(fT_p)|^2 \right\} + \frac{1}{T_f^2} \sum_{m=-\infty}^{\infty} \left| P\left(\frac{m}{T_f}\right) \right|^2 \left| \Phi_{\text{ii}}\left(\frac{mT_p}{T_f}\right) \right|^2 \delta\left(f - \frac{m}{T_f}\right) \quad (2)$$

where

$$\Phi_{\text{ii}}(f) = \sum_{k=0}^{N_s-1} p_k e^{j(2\pi f k)}. \quad (3)$$

2) *Challenges for CCA*: The harsh channel conditions, unique signaling, and strict FCC power limits complicate CCA for I-UWB signals. The channel is an important factor in I-UWB system design. This paper uses the channel model and methodologies from the IEEE 802.15.3a task group [22]. In general, the multipath channel significantly disperses the energy of an I-UWB signal over many paths over possibly hundreds of nanoseconds. Because of the channel, harvesting (and detecting) the full energy of low-power I-UWB signals is even more difficult.

For I-UWB systems at both low and high PRFs, the FCC regulates radiated power, which complicates detection. For systems with a relatively high PRF, the FCC limits the average effective isotropic radiated power (EIRP) to -41.3 dBm/MHz. Because pulses appear more frequently as the PRF increases, the energy of each pulse must be reduced (as compared to

a system with lower PRF) to maintain an equivalent average EIRP. The amplitude of the spectral lines also increases with the PRF; therefore, FCC regulations may further reduce the average power to compensate for the spectral line peaks.

A lower PRF would allow an increased amount of energy per pulse and reduce the spectral line amplitude, but the FCC also regulates the peak power of a single pulse¹ (as opposed to the average EIRP over several PRIs) at low PRFs. This is because the PRF approaches the bandwidth of potential narrowband victim receivers, which may become overloaded. For example, consider a victim receiver with a 1-MHz bandwidth centered on the frequency of peak I-UWB power. The victim would see equal peak and average power from an I-UWB signal with a PRF of 20 MHz. For an I-UWB signal with a PRF of 1 MHz at the same average power, the victim would see a peak power about 7 dB larger than the average power, and the peak to average power ratio further increases with decreasing PRF [23]. Thus, a system designer cannot arbitrarily decrease the PRF to improve the signal-to-noise ratio (SNR).

B. Methods of CCA for I-UWB

I-UWB systems cannot simply detect energy in a certain frequency band; therefore, they must use other methods to perform CCA. Existing methods do not meet our goals of quick, reliable, and efficient detection. We briefly review some existing methods below.

A peak detector is a simple method, which holds the peak value of the signal received within a designated time period. An I-UWB receiver operates over a wide bandwidth; therefore, a peak detector is incapable of separating an I-UWB signal from stronger narrowband signals. This is a problem because I-UWB may overlay many potential narrowband interferers in the 3.1–10.6-GHz range.

A matched filter seems like an ideal method to detect a narrow I-UWB pulse, because it does not require synchronization to detect the signal energy [11]. However, an analog matched filter is not adaptable to dynamic channel conditions and pulse shapes, and its hardware is complex. A digital matched filter requires more complicated hardware, including a fast analog-to-digital converter (ADC) with wide dynamic range. Further, the digital matched filter requires a long training period and a large number of taps. Although suitable for reception, the complexity of a digital matched filter and the inflexibility of an analog matched filter are unsuitable for the purpose of CCA.

Correlation, which is often used to acquire an incoming transmission, can also detect I-UWB activity [11]. Correlation may employ a serial search or a parallel search. In terms of hardware complexity, serial correlation provides the simplest circuit for detection. However, serial correlation is slow (possibly in excess of 1000 symbols) in I-UWB; therefore, it is unsuitable for the purpose of CCA [11]. Parallel correlation improves acquisition speed but at the cost of high circuit complexity; therefore, it is not suitable for CCA. Other methods, such as nonlinear searches or hierarchical searches, also

¹The peak power limit is $20 \log(\text{RBW}/50 \text{ MHz})$ dBm, where RBW is the victim receiver's bandwidth, centered on the UWB peak frequency [25].

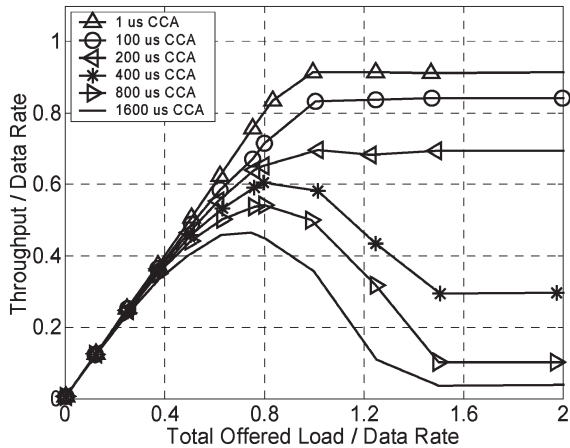


Fig. 1. Network throughput degradation for CSMA as the CCA time increases in an I-UWB network.

improve detection time at the expense of more false alarms and increased variance, and the improvement is still inadequate for the purpose of CCA [24], [25].

An interleaved periodic correlation processing (IPCP) pulse detection system is particularly useful for harvesting the combined energy of all multipaths. IPCP operates by correlating the received signal with samples of itself delayed by one PRI [26]. IPCP is mostly practical for detecting homogenous radar signals. In I-UWB communications systems, the presence of intersymbol interference (ISI), cochannel interference, timing jitter, noise, and modulation (PPM is particularly problematic for IPCP) all produce differences between successive symbols. These differences cause the received signal to be less correlated with a delayed version of itself, which degrades the performance.

C. MAC Protocols

To scale to a large number of nodes, *ad hoc* and sensor networks generally adopt distributed MAC protocols [8], [9], [15]–[17]. In a distributed protocol, each node independently decides to transmit without central guidance. This reduces control overhead, because there is no central synchronization (nor is there a central point of failure). Many *ad hoc* and sensor networks implement distributed medium access with variations of CSMA [18]. In CSMA, CCA (via carrier sense) provides two important services: 1) detecting an incoming packet and 2) checking for a busy channel before transmitting.

Of the I-UWB methods for CCA in the previous section, the most common is serial correlation, because it does not increase hardware complexity like a matched filter, and it is more reliable than a peak detector or IPCP [27]. The simulation results in Fig. 1 show that the long serial correlation time degrades network throughput in a linear network of three nodes A–B–C. All nodes are within range of each other, and A and C transmit 1024-B packets to B at 1 Mb/s. The number of packets per packet time follows a Poisson distribution (hence, packet interarrival times follow an exponential distribution) such that A and C each transmit at an average rate of $0.5 \times$ offered load, where offered load is the rate that data arrives at the MAC layer from an upper layer over all nodes. At 1 Mb/s, a reasonable

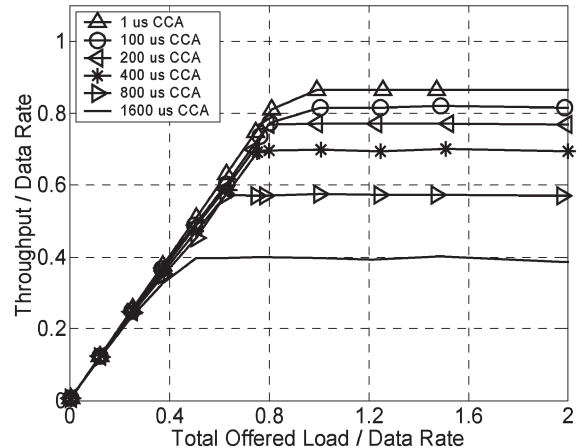


Fig. 2. Throughput degradation for CSMA/CA as the acquisition (CCA) time increases in an I-UWB network.

serial correlation time for I-UWB is between 800 and 1600 μ s (800 to 1600 symbols). Such a long CCA time significantly degrades throughput compared to narrowband CCA times (on the order of a few microseconds at 1 Mb/s), because the information about the state of the medium is outdated and useless. Further, the I-UWB network is unstable, i.e., the throughput decreases as the offered load increases.

To avoid the performance degradation from a long CCA time, distributed MAC protocols may adopt collision avoidance [16]. CSMA with collision avoidance (CSMA/CA) manages collisions through time-duplexed request-to-send (RTS) and clear-to-send (CTS) packets, which provide a virtual CCA [8]. Serial correlation is often used for acquisition, and CSMA/CA must acquire two additional packets for each transaction. The simulation results in Fig. 2 show the throughput degradation of CSMA/CA due to the long acquisition time of the RTS and the CTS packet for an I-UWB radio. Fig. 2 assumes the same configuration as Fig. 1. The CSMA/CA protocol is more stable than CSMA, but I-UWB acquisition times between 800 and 1600 μ s significantly degrade throughput as compared to narrowband acquisition times of around 100 μ s.

Due to the challenges of a distributed approach, most MAC protocols for I-UWB are centralized and target small wireless personal area networks or cellular networks. These centralized MAC protocols do not depend on CCA as the primary means to prevent collisions. Instead, a central controller assigns transmissions to different channels via time division multiple access [28], time hopping codes [29], frequency hopping codes [30], or direct sequence codes [31]. Such approaches are a good strategy for small networks with heavy traffic and strict quality-of-service requirements. However, in large *ad hoc* and sensor networks, the centralized control does not scale well. The control traffic significantly increases overhead, thus wasting bandwidth and energy. Further, because nodes may not be easily serviceable (e.g., battlefields or industrial monitoring), a central failure would render useless thousands of deployed nodes. To avoid central coordination, nodes may determine code channels distributively by the address of the receiver [32] or the sender [33]. However, to prevent simultaneous transmissions to a node, these distributed protocols require control overhead to establish

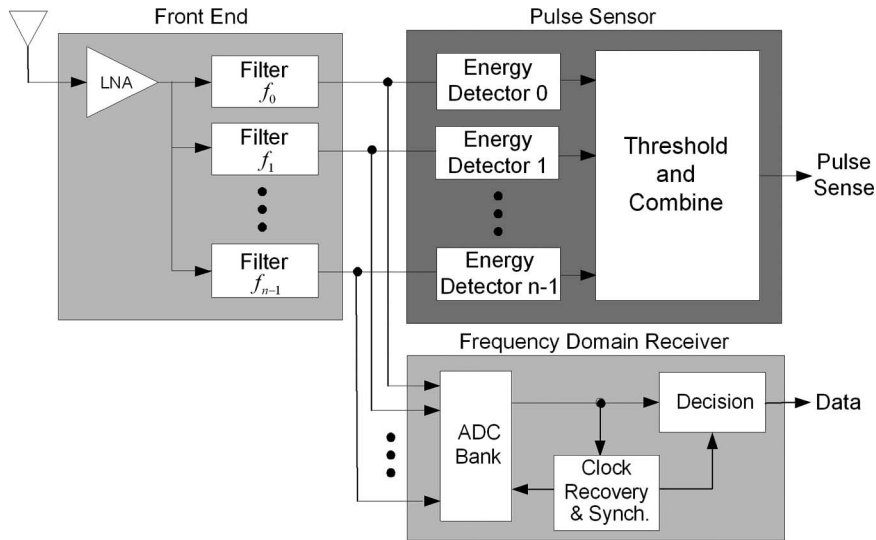


Fig. 3. I-UWB receiver with a pulse sense block.

a link [34], [35]. Further, techniques such as adaptive coding or ignoring corrupted chips are required to mitigate strong multiuser interference [36].

III. ARCHITECTURE AND OPERATION OF THE PULSE SENSOR

Instead of altering I-UWB protocols [29]–[31] to become more distributed, we propose a pulse sensor to enable fundamentally distributed MAC protocols for I-UWB that are similar to CSMA [18]. The proposed pulse sensor is designed to be robust to the weaknesses of the CCA methods in Section II. It detects medium activity quickly, reliably, and efficiently—just as carrier sense detects narrowband signals in a certain frequency band. Instead of searching for a narrow I-UWB pulse over a long time period (as in serial correlation), our pulse sensor examines the signal’s unique spectral power components, which are always present.

A. Architecture

Fig. 3 shows the proposed pulse sensor, which is simple in hardware complexity as compared to a full receiver. The pulse sensor shares the front-end filters with the receiver, and the remaining components of the pulse sensor consume less than 1% of the total layout area of the receiver. Other receiver architectures would require the filters in addition to the pulse sensor. Before explaining the pulse sensor architecture, we briefly describe the overall operation of the receiver in Fig. 3.

The antenna passes the received signal to a wideband low-noise amplifier, which feeds the amplified signal to a bank of typical narrowband resonator filters with the second-order transfer function $1/(s^2 + (k\omega_o)^2)$. A filter captures an in-band spectral component of the received signal at a center frequency of f_i , where $f_i = kF_0$ for an integer k . The fundamental frequency F_0 is determined by an observation period of length T_0 such that $F_0 = 1/T_0$. The receiver supports CMOS im-

plementation through frequency domain sampling, which relaxes the sampling rate of I-UWB signals [14]. Instead of reconstructing the signal from discrete samples in time, spectral samples (each containing a frequency, a phase, and a magnitude) from each filter represent the signal as Fourier coefficients. Filters with narrower bandwidth produce more accurate samples. The ADC captures these spectral samples at the pulse repetition rate, which is much lower than the Nyquist oversampling rate. The decision block performs multipath energy harvesting and baseband signal processing. The clock recovery circuit tracks the optimal point for correlation within a PRI [34].

The receiver components have been fabricated in a 0.18- μm CMOS process for low power dissipation and low cost [35]–[38]. Although the components are not yet integrated, we believe the fabrication and testing shows the feasibility of CMOS implementation. Simulations show that the receiver architecture supports data rates from 1 Kb/s to 1 Gb/s, and it can achieve a bit error rate (BER) of 2×10^{-4} at a 10-m link distance in extreme nonline-of-sight (NLOS) channel conditions at a 100-Mb/s data rate [14]. Lowering the data rate can increase the link distance or improve the BER. Simulations predict 180-mW power dissipation when active (receiving), and common power savings techniques such as reduced ADC resolution or a sleep mode can significantly reduce the power dissipation [39].

The pulse sensor shares the receiver’s filters. When listening (as opposed to actively receiving), the system connects the filter outputs to the pulse sensor instead of the ADC bank. Note that both the receiver and the pulse sensor depend upon filters with narrow bandwidth, which is a desirable characteristic for resonant filters. It may be tempting to design the filters with wide bandwidth to capture as much signal energy as possible, but this approach encounters two challenges for pulse sensing. First, a wideband filter is incapable of separating strong narrowband signals from a weak I-UWB signal. Second, a wideband filter would not respond to the unique regularity of an I-UWB pulse train.

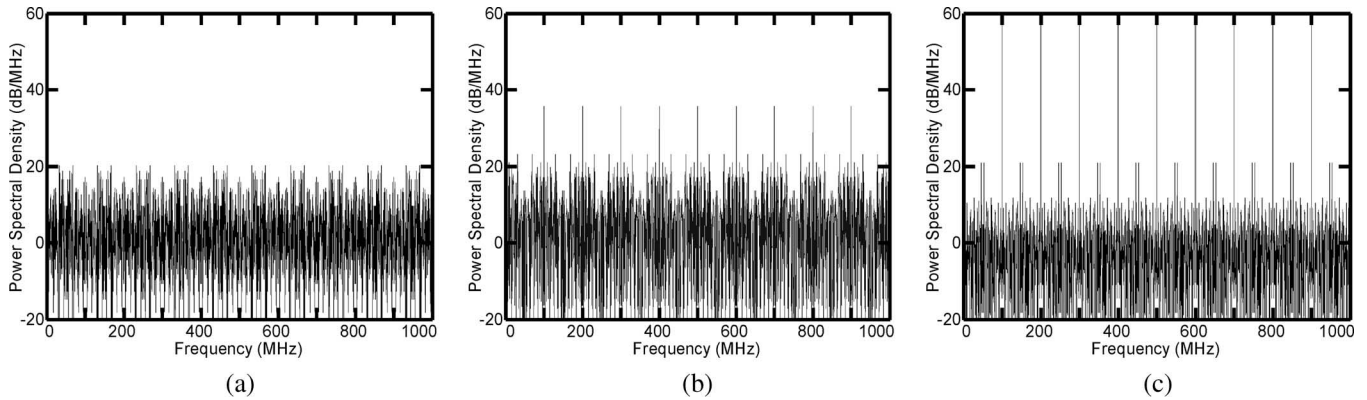


Fig. 4. Line spectrum of 100-MHz PRF BPSK impulse train² with varying information value ratios. (a) Balanced “1” and “-1;” $\mu_i = 0$. (b) 2% more “1” than “-1;” $\mu_i = 0.02$. (c) Squaring circuit; $\mu_i = 1$.

To overcome these challenges, the filter design assumes a power-oriented (as opposed to an energy-oriented) approach. It considers the unique PSD of an I-UWB signal over some time period. From (1) and (2), a regular pulse train creates strong spectral lines around integer multiples of the PRF; therefore, we tune the center frequency of each filter such that $f_i = n\text{PRF}$ for an integer n . (Also, from above, $f_i = kF_0$ for an integer k ; therefore, F_0 should be harmonically related to the PRF.) The pulse sensor then captures energy from the filters when they oscillate at harmonic frequencies of the PRF.

Ideally, the filters would be perfect LC resonators (with an infinite RC time constant), each tuned to an in-band harmonic of the PRF of the impulse train. In any CMOS filter implementation, the finite quality factor Q results in a finite RC time constant and, hence, resonant energy loss over time. Section IV shows that our CMOS filter implementation is sufficient for pulse sensing, because 1) an I-UWB pulse roughly appears as an impulse to the narrowband filters, and 2) the finite Q in the filters results in an RC time constant that attenuates the output response slowly enough to detect the signal energy.

For an RC time constant longer than the PRI, successive antipodal pulses may interfere destructively with each other. In the frequency domain, if an infinite-length BPSK-modulated signal is perfectly balanced in both polarities, then $\mu_i = 0$ in (1), and there is no line spectrum. For a finite-length signal, Fig. 4(a) shows an indiscernible line spectrum for a balanced sequence of impulses² $\delta(t)$ at a 100-MHz PRF. To force a line spectrum, we can inject a running imbalance in the data sequence. Fig. 4(b) shows that just a 2% imbalance produces strong spectral lines with extremely narrow bandwidth. Alternatively, a squaring circuit at the filter input would impose positive pulse polarities, thus forcing $\mu_i = 1$ and producing the strong line spectrum in Fig. 4(c). For OOK or PPM modulation, the above remedies are not necessary, because (1) and (2) guarantee the existence of spectral lines (i.e., nonzero discrete components in the PSD).

An RC time constant shorter than the PRI may be unavoidable in certain technologies. In this case, the destructive

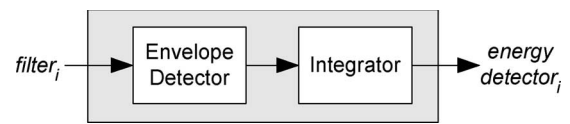


Fig. 5. Energy detector.

interference between successive pulses will be negligible for any modulation.

After the filters capture the line spectrum of a signal, the pulse sensor performs CCA with three additional operations: energy detection, combining, and thresholding. Energy detectors capture the energy of the filter oscillations caused by pulse activity at the PRF. Fig. 5 shows that the implementation of an energy detector can be as simple as an envelope detector followed by an integrator.

Each energy detector reports the presence or absence of a spectral power component at a frequency f_i . The combiner then requires the bulk of these spectral power components to match the low-power footprint of an I-UWB signal. It prevents false alarms from narrowband interference. The level of the threshold detector sets the probability of detection P_d and the probability of false alarm P_{fa} for the I-UWB signal. Our pulse sensor considers two possible methods for combining and thresholding.

Fig. 6(a) shows the first method. The energy detector outputs are applied to threshold detectors, which generate binary values. If the sum of binary values exceeds a value X , then a pulse is detected. This operation is robust to a strong narrowband interferer. High energy in one frequency band cannot singularly exceed X because $X > 1$ (typically, $n = 5$ to 10 filters and $X = \lceil (n + 1)/2 \rceil$). The threshold detectors produce binary values; therefore, the sum and comparator blocks may be implemented efficiently with digital circuits. This option is analogous to a hard decision and is termed hard combination.

Fig. 6(b) shows the second option. The outputs of the energy detectors first pass through limiters so that a strong narrowband interferer does not dictate the final decision. The analog limiter outputs are summed with analog circuitry, and the sum is compared to a threshold. This option produces a more accurate picture of the spectrum, because it weights spectral components according to their strength. The implementation requires only

²We plot the line spectrum of $\delta(t)$ to show (1) independently of pulse shape. $\mathcal{F}\{\delta(t)\} = 1$; therefore, $P(f)$ in (1) = 1, and the figures show only line spectrum.

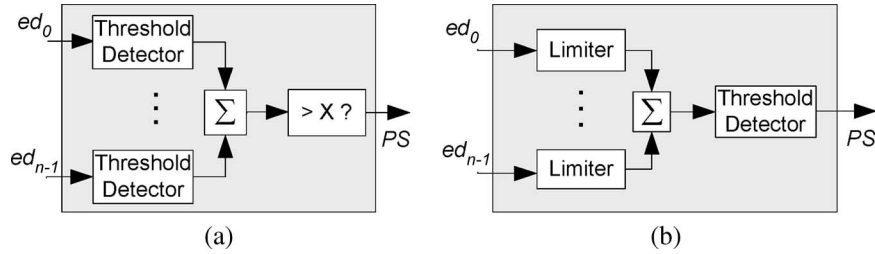


Fig. 6. Combination and threshold blocks. (a) Hard combination. (b) Soft combination.

one threshold detector, but the limiter and the adder circuits are analog to avoid multibit ADC's at the detector input. This option is analogous to a soft decision and is termed soft combination.

B. Operation

This section explains the proper operation of the pulse sensor to ensure a high probability of detection P_d and a low probability of false alarm P_{fa} within a short sensing period. First, to capture the peak oscillation energy, the energy detector in Fig. 5 should integrate for at least one full PRI. This guarantees that the energy detectors capture the peak energy, and it also guarantees that they capture a full filter oscillation. A very fast PRI would be 1 ns (1/1 GHz), and the period $1/f_0$ of the longest filter oscillation can be no longer than 0.32 ns (1/3.1 GHz) to remain in-band. One PRI (symbol) is a short sensing period for any CSMA protocol, e.g., IEEE 802.15.4 specifies an eight symbol maximum [16], and our simulations show that a ten-symbol sensing period does not degrade network throughput. Longer integration periods harvest more signal energy but also increase power dissipation.

Next, for a single integration result, the pulse sensor may decide that a signal is present with a probability distribution of $p_r(x)$ when the signal is actually present with a probability distribution of $p_s(y)$. Thus, the pulse sensor makes a decision with joint probability distribution for $x, y \in [\text{present}, \text{not present}]$. The probability that the circuit decides $x = \text{present}$ when $y = \text{not present}$ is called the probability of false alarm $P_{fa} = P(p_r(x = \text{present}) | p_s(y = \text{not present}))$. The probability distribution $p_s(y)$ is unknown *a priori*, and the circuit decides based upon a constant threshold level. Thus, a false alarm occurs due to noise energy only, and the false alarm probability P_{fa} is constant. Likewise, a detection occurs when the circuit decides $x = \text{present}$ when $y = \text{present}$, and the probability of detection $P_d = P(p_r(x = \text{present}) | p_s(y = \text{present}))$ is constant for a constant threshold level at a given SNR. When choosing the threshold level, a designer usually must decide between reduced collisions (high P_d , high P_{fa}) and full channel utilization (low P_d , low P_{fa}).

The number of "looks" refers to the number of integration results on which the circuit performs the combination and threshold operations. The operations take place at discrete points in time, unlike the continuous time operations of the filters and the energy detector. Multiple looks will increase P_d and decrease P_{fa} at the expense of additional operating time

and power dissipation. Assuming each look is independent, the binomial distribution describes the probability that N false alarms (FAs) or detections (Ds) occur within M looks

$$P(N\text{FAs}) = \binom{M}{N} P_{fa}^N (1 - P_{fa})^{M-N}$$

$$P(N\text{Ds}) = \binom{M}{N} P_d^N (1 - P_d)^{M-N}. \quad (4)$$

We make the following decision rule: A signal is present if it is detected at least N times within M looks. With this decision rule, the cumulative probability distributions are

$$P_{fa}^{\text{cum}} = \sum_{i=N}^M P(i \text{ FAs})$$

$$P_d^{\text{cum}} = \sum_{i=N}^M P(i \text{ Ds}). \quad (5)$$

Considering a practical number of looks to be $M = 3, 5, \text{ or } 7$, we require that $N = \lceil M/2 \rceil$ for detection. Fig. 7(a) and (b) plot P_{fa}^{cum} and P_d^{cum} versus the probability for one look for $[M = 3, N = 2]$; $[M = 5, N = 3]$; and $[M = 7, N = 4]$. The x -axis represents P_d^{cum} or P_d for one look. The y -axis shows the corresponding cumulative probability from (5) over multiple looks. Thus, the plot of $p = p$ designates the probability for one look. For a well-designed system, we expect $P_d > 0.5$ and $P_{fa} < 0.5$; otherwise, the performance is worse than guessing. In Fig. 7(a) for $P_{fa} < 0.5$, the cumulative decision always decreases P_{fa} . The decrease becomes increasingly more significant for lower P_{fa} , e.g., $P_{fa} = 0.1$ for one look and $P_{fa}^{\text{cum}} = 0.0027$ for $[M = 7, N = 4]$. The cumulative decision increases P_d similarly. In general, larger M results in better performance but increases sensing time and power dissipation. We recommend $M = 7$ as a reasonable compromise between detection speed, power, and reliability (high P_d and low P_{fa}).

IV. RESULTS

We performed system level simulations for the pulse sensor in Matlab. The implementation realizes seven filters with center frequencies $f_0 = 4$ GHz, $f_1 = 5$ GHz, $f_2 = 6$ GHz, \dots , $f_6 = 10$ GHz. The circuit parameters are extracted from measurements. The RC time constant is 3 ns in our initial CMOS

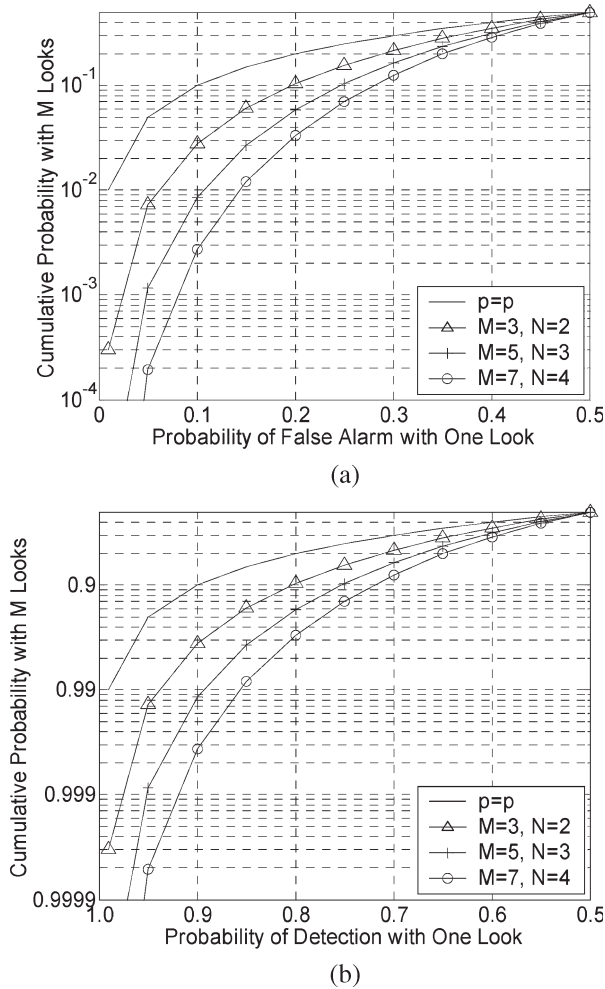


Fig. 7. Cumulative probability distribution of multiple looks compared to a single look. M is the number of looks, and N is the number of detections needed to consider a signal present. The line $p = p$ is the probability for a single look [$M = 1, N = 1$]. (a) Multiple looks decrease P_{fa} . (b) Multiple looks increase P_d .

implementation, and we expect to improve it in future implementations. The PRI is 5 ns, and a rate 1/2 forward error correcting code results in a 100-Mb/s data rate for BPSK and binary PPM modulation. We consider two channel models: CM1 with line-of-sight (LOS) conditions and CM4 with extreme NLOS conditions [22]. Note that the 5-ns PRI can incur significant ISI because the root-mean-square (rms) delay spread is 25 ns for channel model CM4. We vary the E_b/N_0 from 12 to 20 dB, which corresponds to transmitter–receiver distances from 10 to 4 m for an 11-dB noise figure at the antenna terminal as determined by the link budget methodology in [40]. If the PRI increases from the 5 ns baseline, then the link budget will improve by $10 \log_{10}(\text{PRI}'/5 \text{ ns})$ dB, where PRI' represents any PRI longer than 5 ns. The link budget improves until around a 50-ns PRI, when the FCC starts to regulate the peak power of a pulse.

We first derive the theoretical performance of the soft combination scheme in additive white Gaussian noise (AWGN). When passed through a narrowband filter such as the ones in Fig. 3, the noise assumes a Rayleigh distribution [41]. For a fixed threshold voltage V_T , the probability that the noise voltage

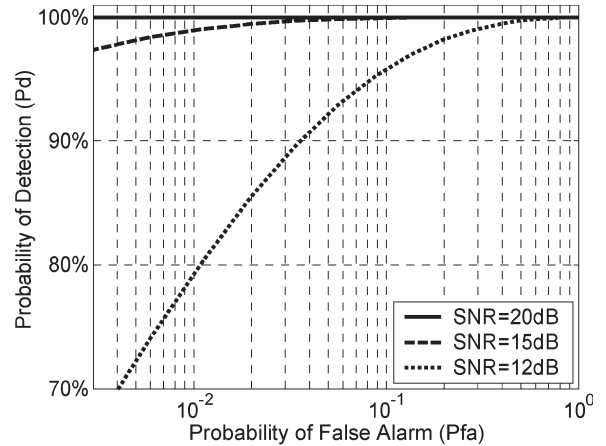


Fig. 8. Analytical P_d versus P_{fa} of our pulse sensor in AWGN.

V_N exceeds V_T , or the probability of a false alarm for one look, is

$$P_{FA} = p(V_N > V_T) = \int_{V_T}^{\infty} \frac{R}{\sigma^2} e^{-\frac{Rr}{2\sigma^2}} dR = e\left(-\frac{V_T^2}{2\sigma^2}\right). \quad (6)$$

When the filters resonate, the output of the filters has a probability density function that includes both the noise V_N and the filter output V_S , and the probability of detection with one look is [41]

$$P_d = p_s(V_S + V_N > V_T) = \int_{V_T}^{\infty} \frac{R}{\sigma^2} e^{-\frac{Rr + A_{eff}^2}{2\sigma^2}} I_0\left(\frac{RA_{eff}}{\sigma^2}\right) dR. \quad (7)$$

The function I_0 is a modified Bessel function of zero order. We denote the effective amplitude of the filter output with A_{eff} , which is determined from the impulse response of the equivalent RLC circuit. In our CMOS implementation, the equivalent RLC circuit attains a neper frequency $\alpha = (2RC)^{-1} \approx 167$ MHz, and the lowest resonant frequency $f_0 = (LC)^{-0.5} = 3.1$ GHz. Thus, all filters are underdamped because $f_i^2 > \alpha^2$ for all i . An underdamped impulse response results in a sinusoid with an exponentially decaying envelope due to the power dissipated in the resistance. Some time after the beginning of a pulse train, the system will reach a steady-state response (i.e., the filter output attains the same maximum voltage V_{max}). At steady state, the effective average amplitude of the signal is

$$A_{eff} = \frac{\int_0^{\text{PRI}} V_{max} e^{-\alpha t} dt}{\text{PRI} \cdot V_{max}} \quad (8)$$

where the envelope of the impulse response of the filter is $V_{max}e^{-\alpha t}$. Note that the effective amplitude increases as the RC time constant ($= 0.5/\alpha$) increases.

Figs. 8–11 demonstrate the proof-of-concept for the pulse sensor. The energy detector takes one look at the filter banks and integrates for 1 PRI or, equivalently, $20/f_0$. The combination scheme is soft combination. Fig. 8 shows the analytical

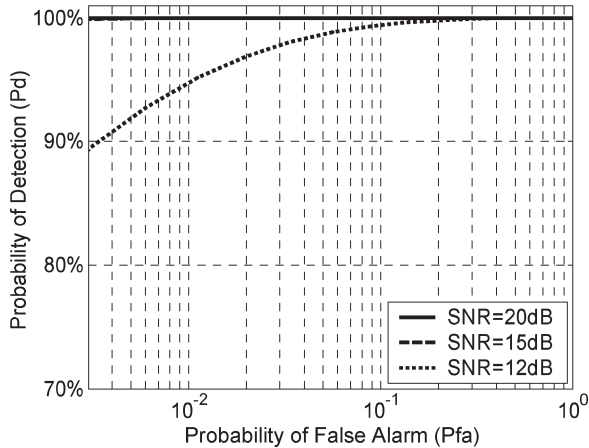


Fig. 9. Analytical P_d versus P_{fa} of our pulse sensor in AWGN with the RC time constant doubled.

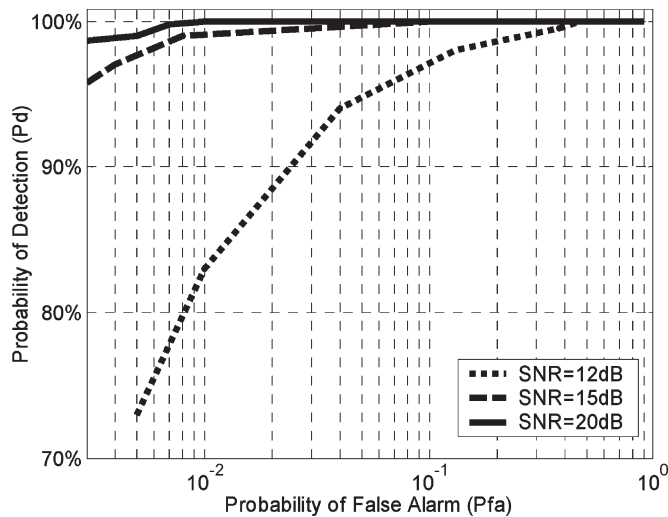


Fig. 10. Simulated P_d versus P_{fa} AWGN.

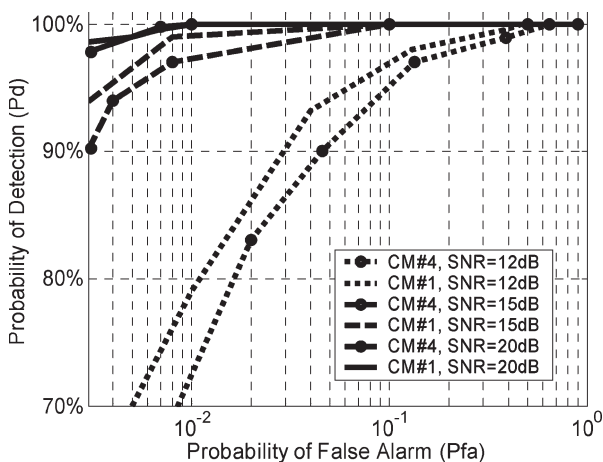


Fig. 11. Simulated P_d versus P_{fa} with multipath channel models CM1 and CM4.

performance in AWGN, and Fig. 9 shows that doubling the RC time constant can significantly improve performance.

Fig. 10 shows the simulated performance in AWGN, and it closely matches the analytical result of Fig. 8. Fig. 11 shows

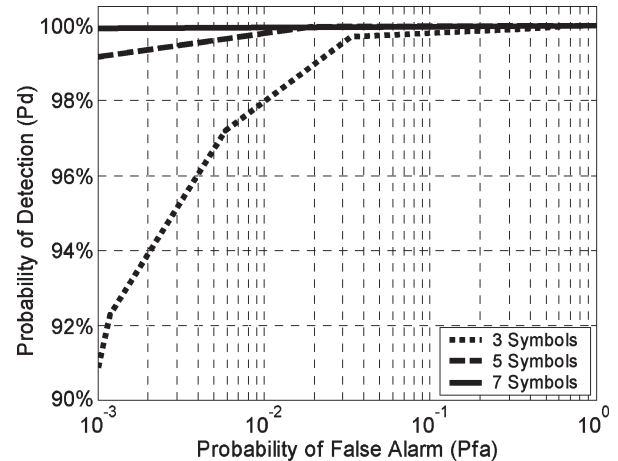


Fig. 12. P_d versus P_{fa} with additional sensing time CM4 $E_b/N_0 = 12$ dB.

the simulated performance under the channel models of CM1 (LOS) and CM4 (extreme NLOS). Note that the addition of the channel model does not significantly degrade performance from the AWGN case. This is because the circuit considers the total spectral energy in the channel; therefore, spreading the total energy over the multipaths does not significantly affect performance. This is a considerable advantage in the dense multipath environment of I-UWB. The pulse sensor performs slightly better in CM1 than CM4, and this is because CM4 may contain multipaths with a large gain as compared to the first path. These multipaths contribute to spectral power at frequencies other than f_i ; therefore, there is some loss in the spectral energy at each f_i .

In the aforementioned simulations, the circuit is practical in all channel conditions for distances 8 m or less ($E_b/N_0 > 15$ dB). For better performance, the pulse sensor could increase three parameters: 1) the RC constant, 2) the integration time, or 3) the number of looks. First, the effects of the RC constant are illustrated in Fig. 9, which shows a significant improvement. However, as noted in Section III, the RC time constant can only be extended as far as the technology allows. Second, if we lengthen the integration time from $1 \cdot \text{PRI}$ to $2 \cdot \text{PRI}$, simulations (not shown in any figure) reveal no significant improvement. This is because of the long baseline integration time (as compared to $1/f_0$), and it suggests that the integration time can be reduced in systems with a PRI less than the RC time constant. Third, Fig. 12 shows that detection probability P_d and false alarm probability P_{fa} can be improved significantly by increasing the number of looks. Note the change of scale on the y -axis. Fig. 12 considers the worst-case channel model of CM4 and an E_b/N_0 of 12 dB. The number of looks M increases to 3, 5, and 7, and the decision is based on the result of the majority of looks $N = \lceil M/2 \rceil$.

Next, Fig. 13 presents the ability of the hard combination and soft combination schemes to reject a strong narrowband interferer. We choose a generic tone interferer [40] because it disturbs the resonator filters more than a modulated signal. We increase the interferer's power level above that in [40] such that the I-UWB signal-to-narrowband-interference ratio is -10 dB [42]. The interferer is centered at 5 GHz to activate filter f_1 . The multipath channel model is the LOS CM1, and the SNR

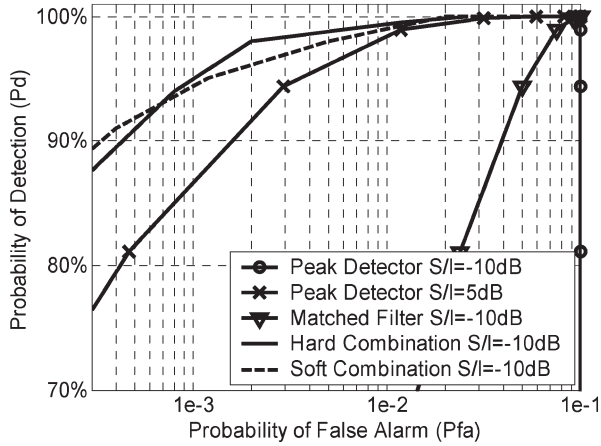


Fig. 13. P_d versus P_{fa} with strong narrowband interferer CM1 $E_b/N_0 = 15$ dB.

is 15 dB. The hard decision block requires four of the seven spectral components to be present, and the limiters constrain the maximum output to 1.8 dB above the average UWB signal level. For either method, the presence of a narrowband signal does not significantly degrade performance compared with other CCA methods.

In Fig. 13, the hard combination method performs best when P_{fa} is relatively high, whereas the soft combination method performs best when P_{fa} is relatively low. The crossover point is around $P_{fa} = 5 \times 10^{-3}$. The reason that hard combination performs best for high P_{fa} is that the threshold value is low; therefore, the narrowband signal may add up to 1.8 dB of energy into the soft combination block, depending on the threshold value. This energy alone may be enough to trigger false alarms and effectively moves the curves in Fig. 13 to the right. However, the narrowband interferer alone cannot change the decision of the hard combination block. At low P_{fa} , the threshold value is high, and therefore, the narrowband interferer cannot add as much energy to the soft combination block. Thus, soft combination yields a better decision. In contrast, the hard combination block continues to weight all inputs—including the interferer—equally at low P_{fa} , so it performs worse than the soft combination block. The hard combination scheme requires far simpler hardware, so it is recommended if its performance is close to that of the soft combination.

Fig. 13 also shows the shortcomings of two of the existing CCA methods for I-UWB in Section II. With an S/I ratio of -10 dB, the peak detector’s false alarm rate is high for any probability of detection. In fact, the P_d versus P_{fa} curve looks like a vertical line on the right of Fig. 13. If the S/I ratio increases by 15 to $+5$ dB, the peak detector performance approaches that of the proposed pulse sensor with an S/I ratio of -10 dB. Next, we simulate an analog matched filter with a transfer function matched to the pulse shape. Although a digital filter could adapt to the channel, it is excessively complex for the purpose of pulse sensing. The matched filter suffers from a low probability of detection, because the channel distorts the pulses and spreads the energy over multiple paths.

Next, we separately consider the effects of timing jitter and multiple transmissions in the channel. Both simulations

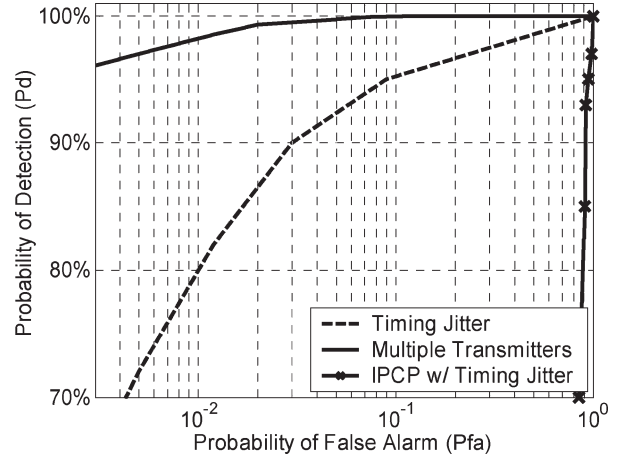


Fig. 14. P_d versus P_{fa} with jitter and multiple transmissions CM1 $E_b/N_0 = 12$ dB.

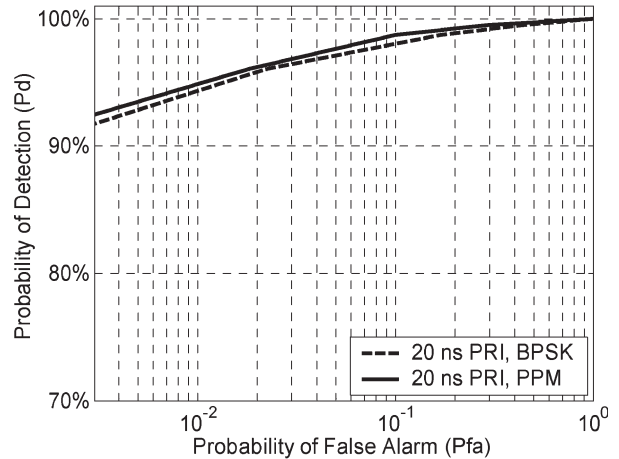


Fig. 15. P_d versus P_{fa} for longer PRI, CM4. Also with PPM modulation.

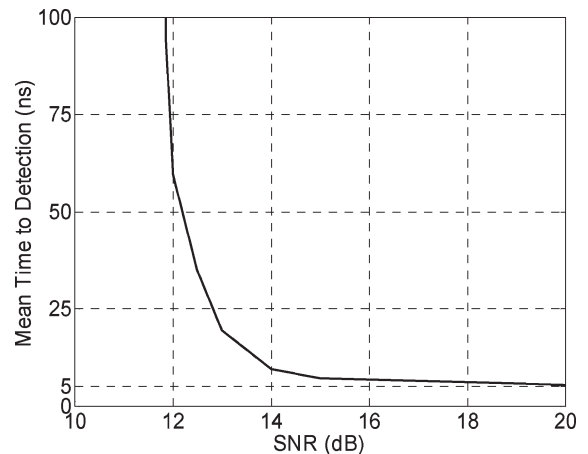


Fig. 16. Mean time to detection versus SNR for a 1-Mb/s data rate in CM4.

consider a 10-m link distance (12 -dB E_b/N_0) in CM1, use soft combination, take one look, and integrate over 1 PRI. The distribution of the jitter is

$$p_\epsilon(x) = \begin{cases} 1/(2\Delta), & -\Delta < x < \Delta \\ 0, & \text{otherwise} \end{cases} \quad (9)$$

TABLE I
SUMMARY OF METHODS TO DETECT MEDIUM ACTIVITY FOR I-UWB

Method	HW Complexity	Speed	Reliability	Notes
Peak Detection	Low	Fast	Unreliable	Interference causes a high false alarm rate
Serial Correlation	Moderate	Slow	Reliable	Long detection time degrades network throughput
Analog Matched Filter	High	Fast	Unreliable	Not adaptable to different channel conditions, pulse distortion, frequency selective fading.
Digital Matched Filter	High	Slow	Reliable	Long training sequence degrades throughput. ADC adds hardware complexity and increases power dissipation.
Parallel Correlation	High	Fast	Reliable	High hardware complexity and power dissipation
IPCP	Moderate	Fast	Unreliable	Timing jitter, noise, and modulation decrease probability of detection. Does not work for orthogonal PPM
CSMA/CA	N/A	Slow	Reliable	Acquisition time of RTS and CTS degrades throughput.
Proposed Pulse Sensor	Low*	Fast	Reliable	Performance degradation as compared to ideal maximum likelihood receiver.

*Low if the pulse sensor can share its filters with the receiver; moderate otherwise.

where $\Delta = 3 \times \text{rms}_{\text{avg}}$, and $\text{rms}_{\text{avg}} = 5$ ps. From Fig. 14, the added jitter shows no visible deterioration from the case without jitter in Fig. 11. This is because the filters capture approximately the same energy, regardless of the jitter. Fig. 14 also shows the drawbacks of the IPCP system in Section II. The delayed signal forms a noisy correlation template that is further corrupted by jitter, ISI, and modulation.

Next, we simulate the performance of the pulse sensor in the presence of multiple transmissions. The circuit sees two transmissions, and one transmission is delayed by a half-PRI with respect to the other. Fig. 14 shows that the performance actually improves, and it is similar to that in Fig. 11 at 15-dB E_b/N_0 , because the energy in the channel is doubled.

The next set of simulations provides some insight into the performance of the pulse sensor at different distances, PRIs, and modulation schemes. The simulations in Fig. 15 use soft combination, integrate over 1 PRI, and operate in CM4.

As the PRI increases, the energy of each pulse can increase while the pulse train maintains the same average power.³ This allows systems to increase either the E_b/N_0 or the range. Fig. 15 shows the results of extending the PRI to 20 ns. This increases the E_b/N_0 by a factor of $10 \log_{10}(20 \text{ ns}/5 \text{ ns}) = 6$ dB; therefore, the resulting E_b/N_0 is 18 dB at 10 m. Note that performance for this longer PRI improves as compared with the performance of the system at 10 m under CM4 in Fig. 11, which has the same average power. Note also that the performance does not improve as if the E_b/N_0 had been increased by 6 dB with a 5-ns PRI. This is because the filters maintain the same 3-ns RC time constant, regardless of the PRI.

Next, we change the modulation scheme to binary PPM with orthogonal pulse positions offset by 1 ns. The simulation conditions are the same as for BPSK with a 20-ns PRI. Fig. 15 shows that the performance of binary PPM closely matches that of BPSK. This is because performance depends more on the total energy in the channel than on the modulation scheme.

To further support our claim of quickly detecting medium activity, we simulate the mean time to detection for a signal with a 5-ns PRI in CM4 under BPSK modulation. The pulse sensor performs one look each PRI, and it decides a signal is present if at least $N = \lceil M/2 \rceil$ out of the last M looks are positive.

³At the PRFs in the simulation, there is room for the PRI to increase without the FCC limiting the peak power of a pulse.

The threshold level results in a P_{fa} of 10^{-3} for one look, and P_{fa} decreases dramatically with more looks, according to (5). Fig. 16 shows that, at our maximum link distance of 10 m (SNR = 12 dB), the system detects the signal in an average of 59.4 ns (11.88 looks). As the SNR increases beyond 12 dB, the detection time converges rapidly to the lowest possible detection time of 5 ns—the time required for one look. Note that an actual system implementation would not behave like the simulation, which increases M and N with time until N detections are reported. Instead, a designer would set M and N *a priori* based on the desired tradeoffs among P_d , P_{fa} , power dissipation, and sensing time. Setting M and N *a priori* prevent the system from detecting weak signals that would not interfere, and it also decreases the probability of false alarm.

Table I summarizes our simulation results for the network (Figs. 1 and 2) and physical layer (Figs. 8–16) performance of our proposed pulse sensor and for the CCA methods from Section II. Recall, we require a pulse sensor to detect medium activity for an I-UWB signal with unknown modulation, channel conditions, phase, and received energy level. Further, the implementation should detect the signal quickly, reliably, and efficiently.

V. CONCLUSION

I-UWB is an attractive radio technology for *ad hoc* and sensor networks. Large *ad hoc* and sensor networks often implement distributed MAC protocols based on CSMA. I-UWB systems have no carrier, and the low duty cycle, low power, strict FCC power limits, and harsh channel conditions further complicate CCA.

We propose a pulse sensor that is the only method in Table I to meet the three critical goals of quickly, reliably, and efficiently performing CCA in an I-UWB network. Simulations and analysis of the proposed architecture show that the pulse sensor is practical. The key idea of the pulse sensor is to examine the spectral power components of an I-UWB signal. Unlike analog matched filtering, the proposed pulse sensor circuit does not rely on a stored template signal; therefore, it does not have to dynamically adapt to changing channel conditions or distortions of the pulse shape. Unlike IPCP, the circuit is insensitive to multipath interference, in-band interference,

ISI, and timing jitter. Further, the pulse sensor can coexist with strong narrowband interferers, whereas a peak detector cannot. The implementation is much less complex than a digital matched filter or parallel correlation, and it does not require sampling or synchronization. Finally, the pulse sensor is faster than digital matched filtering or serial correlation by orders of magnitude.

The proposed pulse sensor enables fundamentally distributed MAC protocols for I-UWB that are analogous to CSMA in narrowband systems. Thus, the pulse sensor allows large *ad hoc* and sensor networks to take full advantage of the benefits of I-UWB radios.

REFERENCES

- [1] S. Verdu, "Spectral efficiency in the wideband regime," *IEEE Trans. Inf. Theory*, vol. 48, no. 6, pp. 1319–1343, Jun. 2002.
- [2] R. J. Fontana, A. Ameti, E. Richley, L. Beard, and D. Guy, "Recent advances in ultra wideband communications systems," in *IEEE UWBST Dig. Papers*, May 2002, pp. 129–133.
- [3] R. Fisher, R. Kohno, H. Ogawa, H. Zhang, M. McLaughlin, and M. Welborn, "DS-UWB physical layer submission to 802.15 task group 3a," *IEEE 802.15-04/137r0*, Mar. 2004. [Online]. Available: [FTP://ftp.802wirelessworld.com/15/04/15-04-0137-00-003a-merger2-proposal-ds-uw-ub-update.pdf](ftp://ftp.802wirelessworld.com/15/04/15-04-0137-00-003a-merger2-proposal-ds-uw-ub-update.pdf)
- [4] A. Batra *et al.*, "Multi-band OFDM Physical Layer Proposal for IEEE 802.15 Task group 3a," *IEEE 802.15-03/268r3*, Mar. 2004. [Online]. Available: <http://www.ieee802.org/15/pub/2003/Jul03/03268r2P802-15-TG3a-Multi-band-CFP-Docment.pdf>
- [5] I. F. Akyildiz, S. Weilian, Y. Sankarasubramaniam, and E. Cayirci, "A survey on sensor networks," *IEEE Commun. Mag.*, vol. 40, no. 8, pp. 102–114, Aug. 2002.
- [6] A. J. Goldsmith and S. B. Wicker, "Design challenges for energy-constrained ad hoc wireless networks," *IEEE Wireless Commun.*, vol. 9, no. 4, pp. 8–27, Aug. 2002.
- [7] D. G. Leeper, "A long-term view of short-range wireless," *Computer*, vol. 34, no. 6, pp. 39–44, Jun. 2001.
- [8] *IEEE Information Technology, Telecommunications and information exchange between systems-Local and metropolitan area networks: Specific requirements—Part 11—Wireless LAN Medium Access Control (MAC) and Physical Layer (PHY) Specifications*, ANSI/IEEE Std 802.11, 1999 ed., 2003.
- [9] M. Leopold, M. B. Dydensborg, and P. Bonnet, "Bluetooth and sensor networks: A reality check," in *Proc. ACM SenSys*, Nov. 2003, pp. 103–113.
- [10] J. R. Foerster, "The performance of a direct-sequence spread ultra-wideband system in the presence of multipath, narrowband interference, and multiuser interference," in *IEEE UWBST Dig. Papers*, May 2002, pp. 91–97.
- [11] V. S. Somayazulu, J. R. Foerster, and S. Roy, "Design challenges for very high data rate UWB systems," in *Conf. Rec. 36th ASILOMAR*, Nov. 2002, vol. 1, pp. 717–721.
- [12] S. Basagni, I. Chlamatac, V. R. Syrotiuk, and B. A. Woodward, "A distance routing effect algorithm for mobility (DREAM)," in *Proc. ACM MOBICON*, Dallas, TX, Oct. 1998, pp. 76–84.
- [13] J. Liu, P. Cheung, L. Guibas, and F. Zhao, "A dual-space approach to tracking and sensor management in wireless sensor networks," in *Proc. ACM WSNA*, Sep. 2002, pp. 131–139.
- [14] H.-J. Lee, D. S. Ha, and H.-S. Lee, "Toward digital UWB radios: Part II—A system design to increase data throughput for a frequency domain UWB receiver," in *Proc. Joint UWBST & UWUWB*, May 2004, pp. 253–257.
- [15] A. Woo and D. E. Culler, "A transmission control scheme for media access in sensor networks," in *Proc. ACM MOBICON*, Jul. 2001, pp. 221–235.
- [16] The Institute of Electrical and Electronics Engineers, Inc., *802.15.4 Standard for Telecommunications and Information Exchange Between Systems*, IEEE Std 802.15.4-2003.
- [17] Y. Wei, J. Heidemann, and D. Estrin, "An energy-efficient MAC protocol for wireless sensor networks," in *Proc. IEEE Infocon*, Jun. 2002, vol. 3, pp. 1567–1576.
- [18] F. Tobagi and L. Kleinrock, "Packet switching in radio channels: Part II—The hidden terminal problem in carrier sense multiple-access and the busy-tone solution," *IEEE Trans. Commun.*, vol. COM-23, no. 12, pp. 1417–1433, Dec. 1975.
- [19] N. J. August, W. C. Chung, and D. S. Ha, "Distributed MAC protocols for UWB ad hoc and sensor networks," in *Proc. IEEE RWS*, Jan. 2006, pp. 511–514.
- [20] J. G. Proakis, *Digital Communications*, 4th ed. New York: McGraw-Hill, 2001.
- [21] M. Z. Win, "Spectral density of random time-hopping spread-spectrum UWB signals with uniform timing jitter," in *Proc. IEEE MILCOM*, Oct. 1999, vol. 2, pp. 1196–1200.
- [22] J. Foerster, "Channel modeling subcommittee report (Final)," *IEEE 802.15 Working Group for Wireless Personal Area Networks (WPANs)*, Tech. Rep. P802.15-02/368r5-SG3a, Dec. 2000. [Online]. Available: <http://grouptr.ieee.org/groups/802/15/pub/2002/Nov02/02490r0P802-15-SG3a-Channel-Modeling-Subcommittee-Report-Final.zip>
- [23] U.S. Federal Communications Commission, *Part 15—Radio Frequency Devices*, Dec. 8, 2003. [Online]. Available: http://www.fcc.gov/oet/inf/rules/part15/part15_12_8_03.pdf
- [24] E. A. Homier and R. A. Scholtz, "Rapid acquisition of ultra-wideband signals in the dense multipath channel," in *IEEE UWBST Dig. Papers*, May 2002, pp. 105–109.
- [25] H. Bing, X. Hou, X. Yang, T. Yang, and C. Li, "A 'two-step' synchronous sliding method of sub-nanosecond pulses for ultra-wideband (UWB) radio," in *Proc. IEEE ICCAS & WESINO Expo*, Jun. 2002, vol. 1, pp. 142–145.
- [26] I. I. Immoreev and D. V. Fedotov, "Detection of UWB signals reflected from complex targets," in *IEEE UWBST Dig. Papers*, May 2002, pp. 193–196.
- [27] J. Ding, L. Zhao, S. Medidi, and K. Sivalingam, "MAC Protocols for ultra-wide-band (UWB) wireless networks: Impact and channel acquisition time," in *Proc. SPIE ITCOM*, Jul. 2002, pp. 97–106.
- [28] The Institute of Electrical and Electronics Engineers, Inc., *802.15.3 Draft Standard for Telecommunications and Information Exchange Between Systems*, Feb. 2003. Draft P802.15.3/D17.
- [29] M. Z. Win and R. A. Scholtz, "Ultra-wide bandwidth time-hopping spread-spectrum impulse radio for wireless multiple-access communications," *IEEE Trans. Commun.*, vol. 48, no. 4, pp. 679–689, Apr. 2000.
- [30] J. Balakrishnan, A. Batra, and A. Dabak, "A multi-band OFDM system for UWB communication," in *Proc. IEEE UWBST*, Nov. 2003, pp. 354–358.
- [31] L. Qinghua and L. A. Rusch, "Multiuser detection for DS-CDMA UWB in the home environment," *IEEE J. Sel. Areas Commun.*, vol. 20, no. 9, pp. 1701–1711, Dec. 2002.
- [32] J.-Y. Le Boudec, R. Merz, B. Radunovic, and J. Widmer, "DCC-MAC: A decentralized MAC protocol for 802.15.4a-like UWB mobile ad hoc networks based on dynamic channel coding," in *Proc. BROADCOM*, Oct. 2004, pp. 396–405.
- [33] M.-G. Di Benedetto, L. De Nardis, M. Junk, and G. Giancola, "(UWB)²: Uncoordinated, wireless, baseborn, medium access control for UWB communication networks," *Mobile Netw. Appl.*, vol. 10, no. 5, pp. 663–674, Oct. 2005.
- [34] N. J. August, H.-J. Lee, and D. S. Ha, "An efficient multi-user UWB receiver for distributed medium access in ad hoc and sensor networks," in *Proc. IEEE RWS*, Sep. 2004, pp. 455–458.
- [35] H.-J. Lee, D. S. Ha, and S. S. Choi, "A systematic approach to CMOS low noise amplifier design for ultra wideband applications," in *Proc. IEEE ISCAS*, May 2005, vol. 4, pp. 3962–3965.
- [36] S. Jose, H.-J. Lee, D. S. Ha, and S. S. Choi, "A low power CMOS power amplifier for ultra wideband (UWB) applications," in *Proc. IEEE ISCAS*, May 2005, vol. 5, pp. 5111–5114.
- [37] R. Thirugnanam, D. S. Ha, and S. S. Choi, "Design of a 4-bit 1.4 Gsamples/s low power folding ADC for DS-CDMA UWB transceivers," in *Proc. IEEE ICU*, Sep. 2005, pp. 536–541.
- [38] S. Wang, D. S. Ha, and S. S. Choi, "Design of a 6-bit 5.4-Gsamples/s CMOS D/A converter for DS-CDMA UWB transceivers," in *Proc. IEEE ICU*, Sep. 2005, pp. 333–338.
- [39] H.-J. Lee, D. S. Ha, and H.-S. Lee, "Toward digital UWB radios: Part I—Frequency domain UWB receiver with 1 bit ADCs," in *Proc. Joint UWBST & IWUWB*, May 2004, pp. 248–252.
- [40] J. Ellis, K. Siwiak and R. Roberts, "P802.15.3a Alt PHY selection criteria," *IEEE P802-15_03031r11_TG3a-PHY-Selection-Criteria*, May 18, 2003. [Online]. Available: http://grouptr.ieee.org/groups/802/15/pub/2003/May03/03031r11P802-15_TG3a-PHY-Selection-Criteria.doc
- [41] M. L. Skolnik, *Introduction to Radar Systems*, 2nd ed. New York: McGraw-Hill, 1980.
- [42] M. Hamalainen, V. Hovinen, R. Tesi, J.H.-J. Iinatti, and M. Latva-aho, "On the UWB system coexistence with GSM900, UMTS/WCDMA, and GPS," *IEEE J. Sel. Areas Commun.*, vol. 20, no. 9, pp. 1712–1721, Dec. 2002.



Nathaniel J. August (M'03) was born in Maryland in 1975. He received the B.S. degree in computer engineering with a minor in computer science, the M.S. degree in electrical engineering, and the Ph.D. degree in electrical engineering from Virginia Tech, Blacksburg, in 1998, 2001, and 2005, respectively.

He has worked as a Validation Engineer for Intel Corporation, Folsom, CA, and in Portland, OR, during internships from 1995 to 2005. He is currently a Mixed-Signal Component Design Engineer for Intel Corporation, Portland. He has published ten IEEE papers in the field of ultrawideband (UWB) communication, and he is a coauthor of the recent book *An Introduction to Ultra Wideband Communication Systems* (Prentice-Hall, 2005). His research interests include low-power very large scale integration (VLSI) design, video codecs, signal processing, radio frequency identification (RFID) systems, and UWB communications systems.



Hyung-Jin Lee (M'03) was born in Seoul, Korea, in 1973. He received the B.S. degree in electrical engineering from Hanyang University, Seoul, in 2000 and the M.S. and Ph.D. degrees in electrical engineering from Virginia Tech, Blacksburg, in 2003 and 2006, respectively.

From 2000 to 2006, he was with the Virginia Tech VLSI for Telecommunications (VTVT) Laboratory, where he researched low-power high-performance CMOS radio frequency integrated circuit (RFIC) design, high-speed CMOS analog integrated circuit design, and system-level architectures targeted for UWB CMOS communication systems. Since March 2006, he has been a Senior RFIC Design Engineer for Intel Corporation, Portland, OR.



Dong Sam Ha (M'86–SM'97) received the B.S. degree in electrical engineering from Seoul National University, Seoul, Korea, in 1974 and the M.S. and Ph.D. degrees in electrical and computer engineering from University of Iowa, Iowa City, in 1984 and 1986, respectively.

Since Fall 1986, he has been a faculty member with the Department of Electrical and Computer Engineering, Virginia Tech, Blacksburg. Currently, he is Professor and Director of the Center for Embedded Systems and Critical Applications. He supervises the VTVT group, which specializes in VLSI design for wireless communications. During a research leave from January to June 2003, he worked for Freescale, where he was involved in UWB system design. Along with his students, he has developed four computer-aided design tools for digital circuit testing and has created a standard library of CMOS cells. The library cells and the source code for the four tools have been distributed to over 250 universities and research institutions worldwide. He contributed to the recent book *An Introduction to Ultra Wideband Communication Systems* (Prentice-Hall, 2005) and has published 30 papers in the UWB area over the past three years. His research interests include low-power VLSI design for wireless communications, low-power/high-speed analog and mixed-signal design, RF IC design, UWB RFIDs, wireless sensor systems, and reconfigurable architectures.

Dr. Ha was General Chair of the System-on-Chip Conference in 2005 and a member of the Technical Program Committee of the International Conference on Ultra Wideband in 2005.